ARTICLE

Observation of Interference Effects in (e, 2e) Electron Momentum Spectroscopy of SF_6

Min-fu Zhao[a,b], Xu Shan[a]*, Jing Yang[a], En-liang Wang[a], Shan-shan Niu[a], Xiang-jun Chen[a]

a. Hefei National Laboratory for Physical Sciences at the Microscale and Department of Modern Physics, University of Science and Technology of China, Hefei 230026, China
b. The Center of Basic Laboratory, West Anhui University, Lu'an 237012, China

(Dated: Received on August 9, 2015; Accepted on August 20, 2015)

Two-dimensional electron density map (2D map) of binding energy and relative azimuthal angle (*i.e.*, momentum) for the outer-valence molecular orbitals of SF_6 has been measured by a highly sensitive electron momentum spectrometer with noncoplanar symmetric geometry at the impact energy of 1.2 keV plus binding energy. The experimental electron momentum profiles for the relevant molecular orbitals have been extracted from the 2D map and interpreted on the basis of the quantitative calculations using the density functional theory with B3LYP hybrid functional. For the outermost F2p nonbonding orbitals of SF_6, the interference patterns are clearly observed in the ratios of the electron momentum profiles of molecular orbitals to that of atomic F2p orbital.

Key words: (e, 2e) electron momentum spectroscopy, Interference effect, Bond oscillation, Electron momentum profile

I. INTRODUCTION

Electron momentum spectroscopy (EMS), also known as binary (e, 2e) spectroscopy, is a powerful technique for exploring the electronic structures of atoms and molecules [1−4]. The principal value of the EMS for understanding the electron behavior lies in its unique ability to measure the electron density distribution in momentum space (p-space) for the ionized orbital, which is directly proportional to the square modulus of the wavefunction ($|\psi(\mathbf{p})|^2$). For molecules, the orbital wavefunction in position space (r-space) can be approximated as a linear combination of atomic orbitals (AOs), *i.e.*,

$$\psi(\mathbf{r}) = \sum_{J=1}^{N} c_J \phi_J(\mathbf{r} - \mathbf{R}_J) \tag{1}$$

where $\mathbf{R}_J$ is the position of Jth atom. The corresponding wavefunction in p-space can thus be obtained according to the Dirac-Fourier transform, *i.e.*,

$$\psi(\mathbf{p}) = \sum_{J=1}^{N} \exp(-i\mathbf{p}\cdot\mathbf{R}_J) \times c_J \phi_J(\mathbf{p}) \tag{2}$$

here, $\exp(-i\mathbf{p}\cdot\mathbf{R}_J)$ is the phase factor, in which the information on molecular geometry is involved. Therefore, the EMS cross section, $\sigma \propto \int \mathrm{d}\Omega |\psi(\mathbf{p})|^2$, is subjected to a modulation of the cosinusoidal or sinusoidal function, and should exhibit an oscillation behavior. Such oscillation phenomenon is called bond oscillation which is the result of interference effect. It has been firstly discussed in the 1980s [5, 6], but due to the limitation of the performance of traditional EMS spectrometer, it was only observed very recently in EMS experiments on CF_4 [7] and H_2 [8, 9]. To our knowledge, no other EMS studies are reported so far on this aspect and further investigations are expected for the extensive species, especially for the relatively complicated molecules.

In the present work, we choose SF_6 molecule as a target, which is characterized by an octahedral structure and owns two kinds of F−F bond lengths. Like CF_4 [7], the first four outer-valence molecular orbitals (MOs) of SF_6 are essentially F2p lone pairs. This may bring visible interference effects in the electron momentum density distributions of MOs. The previous EMS experiments on SF_6 [10, 11] focused on the study of electronic structures including the assignments of ionization bands to the specific MO levels in dispute. Unfortunately, subject to the low statistics of EMS measurement at that time, it was quite difficult to observe the interference effect. In the present work, benefited from our latest version of EMS spectrometer [12], a significant improvement of the statistical accuracy has been achieved and the interference patterns in the electron momentum density distributions are clearly observed for the outermost F2p nonbonding orbitals of SF_6.

*Author to whom correspondence should be addressed. E-mail: xshan@ustc.edu.cn

II. EXPERIMENTAL AND THEORETICAL BACKGROUND

EMS is based on the kinematically complete (e, 2e) process, in which a high-energy incident electron is scattered by the target atom or molecule and a target electron is cleanly knocked out simultaneously. The present experiment on SF_6 is carried out by using a high-sensitivity EMS spectrometer which was described in detail elsewhere [12], and only a brief description is given here. The typical energy of the incident electron is 1.2 keV plus binding energy. In the employed symmetric non-coplanar kinematics, the ejected and scattered electrons with equal polar angles (θ_a=θ_b=θ=45°) and energies (E_a=E_b) are analyzed by a 90° sector, 2π spherical electrostatic analyzer. The two electrons are then detected in coincidence by a position sensitive detector with double-half wedge-strip anode (DH-WSA PSD) placed at the exit plane of the analyzer. Considering conservation of energy and momentum, the binding energy ε and magnitude of momentum p of target electron can be expressed as

$$\varepsilon = E_0 - E_a - E_b \tag{3}$$

$$p = \left\{ (2p_a \cos\theta - p_0)^2 + \left[2p_a \sin\theta \sin\left(\frac{\phi}{2}\right) \right] \right\}^{1/2} \tag{4}$$

where (E_0, p_0), (E_a, p_a) and (E_b, p_b) are the energies and momenta of the projectile, scattered and ejected electrons, respectively. And ϕ is the relative azimuthal angle between the two outgoing electrons. Before the experiment of SF_6, the energy and momentum resolutions of the present EMS spectrometer are determined to be ~1.5 eV (full width at half maximum (FWHM)) and ~0.2 a.u., respectively, by measuring the binding energy spectrum and electron momentum distribution of Ar3p orbital.

On the theoretical side, within the binary encounter approximation and the plane wave impulse approximation (PWIA), as well as the target Hartree-Fock (HF) or Kohn-Sham (KS) approximation, the triple differential cross-section (TDCS) of (e, 2e) process can be described as [1−4]:

$$\sigma_{\rm EMS} = (2\pi)^4 \frac{p_a p_b}{p_0} f_{ee} \times \frac{1}{4\pi} S_i^{(f)} \int {\rm d}\Omega |\psi_i(\mathbf{p})|^2 \tag{5}$$

where f_{ee} is the Mott-scattering cross section for electrons and $\psi_i(\mathbf{p})$ is the one-electron canonical HF or KS wavefunction in momentum space for the ith orbital from which the electron is knocked out. $S_i^{(f)}$, known as spectroscopic factor or pole strength, denotes the possibility of forming a one-hole configuration in the final state f. The integral in Eq.(5) is usually referred to as the spherically averaged one-electron momentum distribution, *i.e.*, electron momentum profile.

For SF_6 molecule, the first four MOs are essentially composed of F2p AOs, and similar to the case of CF_4 [7, 13], each can be described as

$$\psi_i(\mathbf{r}) = \sum_{J=1}^{6} c_J \phi_{2p}(r_J) \left[\sum_{m=-1}^{1} a_{J,m} Y_{1,m}(\Omega_{\mathbf{r}_J}) \right] \tag{6}$$

where c_J is the expansion coefficient, $\phi_{2p}(r_J)$ is the radial part of F2p AO located at Jth F atom position $\mathbf{R}_J$, and $\mathbf{r}_J$=$\mathbf{r}$−$\mathbf{R}_J$. $Y_{1,m}$ denotes spherical harmonics with the orbital angular momentum quantum number l=1 and magnetic quantum number m. The coefficient $a_{J,m}$ satisfies $\sum_{m=-1}^{1} |a_{J,m}|^2$=1.

Correspondingly, the MOs in p-space is given by

$$\psi_i(\mathbf{p}) = \sum_{J=1}^{6} \exp(-i\mathbf{p}\cdot\mathbf{R}_J) \cdot \int {\rm d}\mathbf{r} (2\pi)^{-3/2} \exp(-i\mathbf{p}\cdot\mathbf{r}_J) c_J \phi_{2p}(r_J) \cdot \left[\sum_{m=-1}^{1} a_{J,m} Y_{1,m}(\Omega_{\mathbf{r}_J}) \right] \tag{7}$$

The exponential term of $\exp(-i\mathbf{p}\cdot\mathbf{r}_J)$ in Eq.(7) can be expanded by using spherical harmonics, *i.e.*,

$$\exp(-i\mathbf{p}\cdot\mathbf{r}_J) = 4\pi \sum_{l,m} (-i)^l j_l(pr) {\rm Y}^*_{l,m}(\Omega_{\mathbf{r}_J}) {\rm Y}_{l,m}(\Omega_{\mathbf{p}}) \tag{8}$$

where $j_l(pr)$ is the spherical Bessel function with order l.

Therefore Eq.(7) is simplified to

$$\psi_i(\mathbf{p}) = \phi_{2p}(p) \sum_{J=1}^{6} c_J \exp(-i\mathbf{p}\cdot\mathbf{R}_J) \cdot \left[\sum_{m=-1}^{1} a_{J,m} Y_{1,m}(\Omega_{\mathbf{p}}) \right] \tag{9}$$

$$\phi_{2p}(p) = \sqrt{\frac{2}{\pi}} (-i)^1 \int j_1(pr) \phi_{2p}(r) r^2 {\rm d}r \tag{10}$$

where $\phi_{2p}(p)$ is the radial part of F2p in p-space.

By substituting Eq.(9) into Eq.(5), the EMS cross section for MOs can be further deduced to be [7, 13]

$$\sigma_{\psi_i}(p) = \sigma_{F2p}(p) S_i^{(f)} a_0 \left[1 + \sum_{J\neq K} a_{1J} j_0(pR_{JK}) + \sum_{J\neq K} a_{2J} j_2(pR_{JK}) \right] \tag{11}$$

where $\sigma_{F2p}(p)$ is the cross section for F2p AO, R_{JK} represents the distance between two F atoms and a_0, a_{1J}, a_{2J} are constants which depend on the coefficients and components of AOs used to compose the MO. For different MOs, these constants are essentially different.

DOI:10.1063/1674-0068/28/cjcp1508168

One can see from Eq.(11) that the EMS cross section of MOs is modulated by the factor F_{ψ_i},

$$F_{\psi_i}=a_0\left[1+\sum_{J\neq K}a_{1J}j_0(pR_{JK})+\sum_{J\neq K}a_{2J}j_2(pR_{JK})\right] \quad (12)$$

which governs the oscillatory behavior, so F_{ψ_i} is referred to as the interference factor.

In the present calculations, based on the molecular geometry of SF_6 optimized by the second-order Møller-Plesset perturbation (MP2) [14] method with aug-cc-pVTZ basis set [15], the MO wavefunctions in r-space are calculated at the theoretical levels of HF [1−4] and B3LYP [16−19] with 6-311++G** and aug-cc-pVTZ basis sets. Thus, the theoretical electron momentum profiles for the outer-valence MOs of SF_6 are obtained according to Eq.(5). All the theoretical calculations are carried out using the Gaussian 03 suite of programs [20].

III. RESULTS AND DISCUSSION

A. Binding energy spectra

SF_6 molecule has 70 electrons and belongs to O_h point group. Its ground state electronic configuration can be written as [11, 21]

$$(\text{core})^{22}\underbrace{(4a_{1g})^2\,(3t_{1u})^6\,(2e_g)^4\,(5a_{1g})^2}_{\text{Inner-valence}}$$
$$\underbrace{(4t_{1u})^6\,(1t_{2g})^6\,(3e_g)^4\,(5t_{1u})^6\,(1t_{2u})^6\,(1t_{1g})^6}_{\text{Outer-valence}}$$

Note that $1t_{2u}$ and $5t_{1u}$ are almost degenerate in energy, and the corresponding ionization bands cannot be separated even by high-resolution photoelectron spectroscopy (PES) [21].

Figure 1(a) shows the two-dimensional electron density map (2D map) of binding energy and relative azimuthal angle (*i.e.*, momentum) for SF_6 obtained by the high-sensitivity EMS spectrometer [12] with the simultaneous measurement of energy and momentum in the desired ranges. This 2D map contains the information on energy distributions (binding energy spectra), momentum distributions, and symmetries for various ionization states. The total binding energy spectrum (BES), as shown in Fig.1(b), is obtained by summing up intensities over the entire range of relative azimuthal angles in the 2D map. Three envelopes are observed in the BES in the outer-valence region. The first envelope corresponds to the ionizations from the outermost four MOs, $1t_{1g}$, $1t_{2u}$, $5t_{1u}$, and $3e_g$, each of which is composed of F2p AOs. The second and third ones correspond to the ionizations from $1t_{2g}$ and $4t_{1u}$ MOs.

In order to extract experimental electron momentum profiles (XMPs) for the outer-valence MOs, the deconvolution of the BES for each of a chosen set of angles

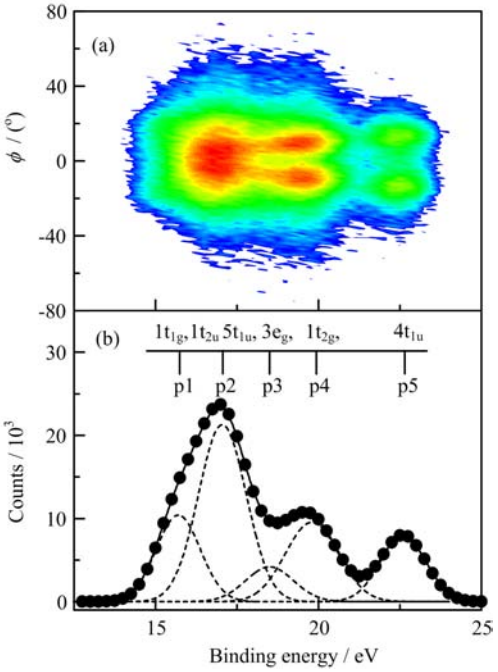

FIG. 1 (a) Two-dimensional density map of binding energy and relative azimuthal angle of SF_6. (b) Total binding energy spectrum of SF_6. The dashed curves represent the Gaussian deconvolution functions and the solid curve is their sum. Vertical bars indicate the ionization energies of the outer valence orbitals.

ϕ has been performed by least-squares fitting. Five Gaussian functions are used to fit the BES as shown by the dashed curves in Fig.1(b) and the overall fitting is represented by the solid line. The positions of Gaussian peaks (p1−p5) are referred to the ionization energies obtained by the high-resolution PES [21], and the widths are the combination of EMS instrumental energy resolution and Franck-Condon widths of the ionization bands deduced from the PES [21]. The first peak (p1) at 15.7 eV corresponds to $1t_{1g}$ MO. The second one (p2) at 17.1 eV is associated with two almost degenerate MOs of $1t_{2u}$ and $5t_{1u}$. The third one (p3) at 18.5 eV is relevant to $3e_g$, and the last two peaks (p4 at 19.8 eV and p5 at 22.6 eV) correspond to $1t_{2g}$ and $4t_{1u}$, respectively.

B. Experimental and theoretical electron momentum profiles

The XMPs for each of peaks (p1−p5) are extracted by plotting area under the corresponding fitted peaks as a function of momentum p (*i.e.*, angle ϕ). The theoretical electron momentum profiles (TMPs) for the outer-valence MOs of SF_6 are calculated using HF and B3LYP methods with basis sets of 6-311++G** and aug-cc-pVTZ. For the sake of comparison, the TMPs have been folded with the instrumental momentum resolution using the Gaussian weighted planar grid method

DOI:10.1063/1674-0068/28/cjcp1508168

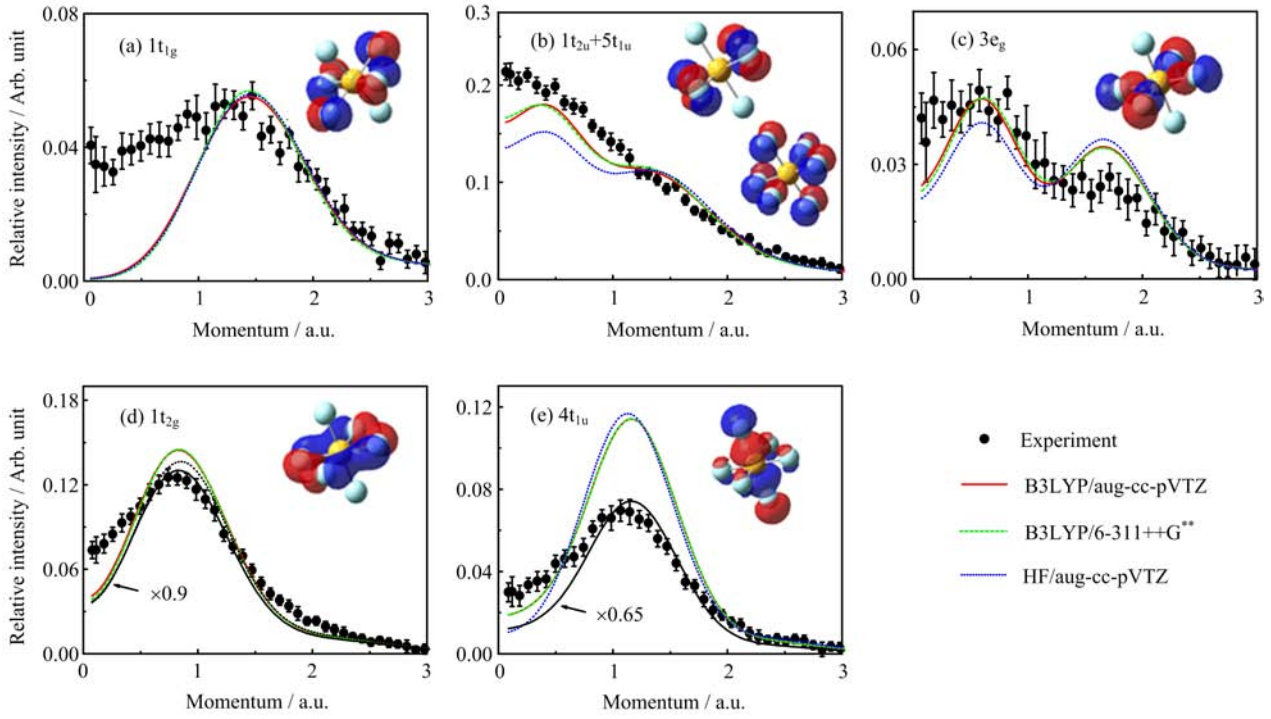

FIG. 2 The XMPs and the TMPs for outer-valence orbitals: (a) $1t_{1g}$, (b) $1t_{2u}$+$5t_{1u}$, (c) $3e_g$, (d) $1t_{2g}$, and (e) $4t_{1u}$. The TMPs are calculated by HF and B3LYP methods with 6-311++G** and aug-cc-pVTZ basis sets within the PWIA approximation. The orbital maps in r-space are calculated by B3LYP/aug-cc-pVTZ.

[22]. Furthermore, the XMPs and the TMPs are placed on a common intensity scale using a universal factor obtained by normalizing the summed XMPs for p1, p2, p3, and p4 to the summed TMPs for $1t_{1g}$, $1t_{2u}$, $5t_{1u}$, $3e_g$, and $1t_{2g}$. The XMPs and the corresponding TMPs for the outer-valence MOs of SF_6 are shown in Fig.2. It is noted that the error bars of experimental data given in the figures represent the overall error of the statistical and deconvolution uncertainties. In addition, the molecular orbital maps in r-space calculated by B3LYP/aug-cc-pVTZ are also illustrated in Fig.2.

Figure 2(a) shows the XMP and the TMPs for $1t_{1g}$ which is composed of four F2p AOs as the orbital map displays. The XMP shows a "p-type" character with a maximum at $p\approx1.5$ a.u., and a distinct "turn up" appears at $p<1$ a.u. All the calculations within the PWIA approximation predict the same "p-type" TMPs, but largely underestimate the intensity at $p<1$ a.u. Figure 2(b) compares the XMP with the summed TMPs for two almost degenerate MOs $1t_{2u}$ and $5t_{1u}$ which are dominated by two and three pairs of F2p AOs, respectively. The TMPs describe the XMP qualitatively except for the intensity at low momentum. Figure 2(c) depicts the XMP and TMPs for $3e_g$ MO which is also dominated by two pairs of F2p AOs. The XMP and TMPs both exhibit double "p-type" character with one maximum at $p\approx0.6$ a.u. and the other at $p\approx1.7$ a.u. A reasonable agreement between XMP and TMPs is observable. Figure 2 (d) and (e) show the XMPs for $1t_{2g}$ and $4t_{1u}$, respectively. The orbital maps show that these two orbitals are predominantly F2p lone pairs with a little admixture of sulfur components. The XMPs and the corresponding TMPs both display "p-type" feature, and all the TMPs overestimate the XMPs. When the TMPs are scaled by proper factors, general agreements can be achieved except in the low momentum region. The obtained factors, 0.9 for $1t_{2g}$ and 0.65 for $4t_{1u}$, are essentially the pole strengths for the ionizations. The evidence of pole strength splits for the ionizations from $1t_{2g}$ and $4t_{1u}$ was predicted by the calculation of Weigold *et al.* using the third-order algebraic diagrammatic construction method [11].

It is worthwhile to note that the XMPs for all the outer-valence MOs of SF_6 show obviously higher intensity than the TMPs in the low momentum region ($p<1$ a.u.). This finding is consistent with the previous EMS results of Weigold *et al.*, who suggested that the observed discrepancies may be due to the inadequacy of basis sets or the initial state correlations [11]. However, the present calculations using larger basis sets and the density functional theory with B3LYP hybrid functional, which take into account initial state correlation to some extent, do not improve the agreement, indicating that other physical reasons should be considered. One possible reason is the distorted wave effect, which was proposed by Brion *et al.* [23] to explain the observed high intensity in the low momentum region of the electron momentum profiles for atomic d orbitals,

DOI:10.1063/1674-0068/28/cjcp1508168

as well as for d-like or π^*-like molecular orbitals that exhibit gerade symmetry [23−26]. The orbital maps in Fig.2 indicate that the outer-valence MOs of SF_6 all display π^*-like characteristic. Another possible reason is the vibrational effect as revealed by some recent EMS studies that the vibrational motions of initial state of polyatomic molecule may substantially change the electron momentum profiles in the low momentum region [27−30]. The contamination from the nearby ionization bands due to severe overlaps may also contribute to the discrepancies.

C. Interference effects

As described above, for the outermost four nonbonding MOs of SF_6 dominated by F2p lone pairs, the EMS cross section ($\sigma_{\psi_j}(p)$) can be expressed as the product of the cross section of F2p AO ($\sigma_{\mathrm{F2p}}(p)$) and the interference factor (F_{ψ_j}) according to Eq.(11). Therefore the interference pattern can be observed through dividing the cross section of MO by that of F2p AO. Taking into account the possible distorted wave effect, $\sigma_{\mathrm{F2p}}(p)$ is calculated with the distorted-wave Born approximation (DWBA) method [31] using B3LYP/aug-cc-pVTZ wavefunction. The calculated $\sigma_{\mathrm{F2p}}(p)$ is also folded with the present instrumental momentum resolution.

Figure 3 shows the ratios of the XMPs for $1t_{1g}$, $1t_{2u}$+$5t_{1u}$, and $3e_g$ MOs to the TMP for F2p AO calculated by the DWBA, together with the theoretical ratios of the TMPs for MOs to that of F2p AO which are both calculated using B3LYP/aug-cc-pVTZ within the PWIA. One can see from the figure that the oscillation structures are observed clearly in both the experimental and theoretical ratios. In order to confirm the interference effect, the interference factors F_{ψ_j} for different orbitals are also plotted in Fig.3. To calculate the interference factors, S−F bond length (R_{SF}=2.95 a.u.) from the electron diffraction [32] is employed. The calculated values for coefficients a_{1J} and a_{2J} of the zero and second order spherical Bessel functions are fixed, while a_0 is determined by best fitting to the experimental ratio. It can be seen from Fig.3 that the observed oscillatory structures can readily be described by the interference factors, indicating unambiguously the presence of interference effect or bond oscillation. In addition, the discrepancies between experimental and theoretical ratios in the low momentum region still exist, especially for $1t_{1g}$ orbital. The distorted wave effect could no longer be responsible for it because such an effect involved in the cross sections should largely be eliminated in the cross section ratios. Therefore, the vibrational effect as well as the contamination from nearby ionization bands may contribute to the discrepancies. In order to eliminate the possible deconvolution uncertainty, we also plot the experimental and theoretical ratios for the summation of the four outermost MOs in Fig.4, together

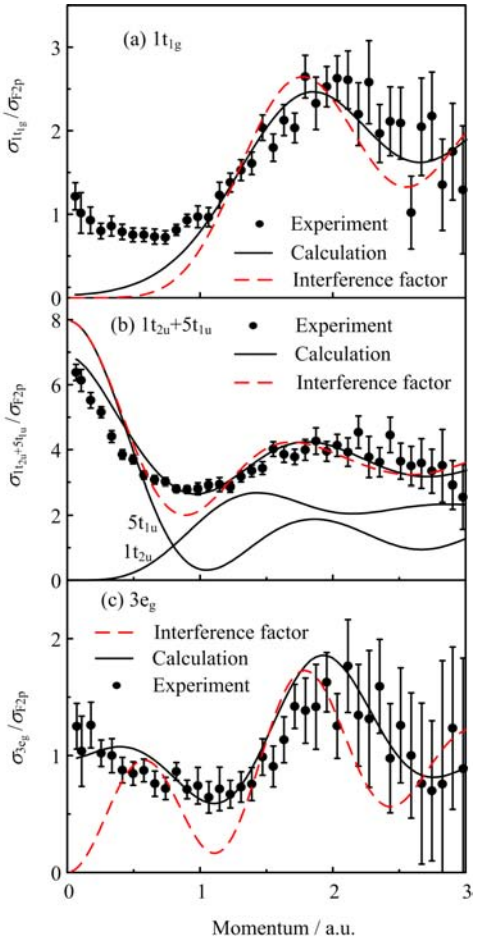

FIG. 3 Ratios of EMS cross sections of MOs to that of F2p AO and the corresponding interference factors for (a) $1t_{1g}$, (b) $1t_{2u}$+$5t_{1u}$, and (c) $3e_g$ of SF_6.

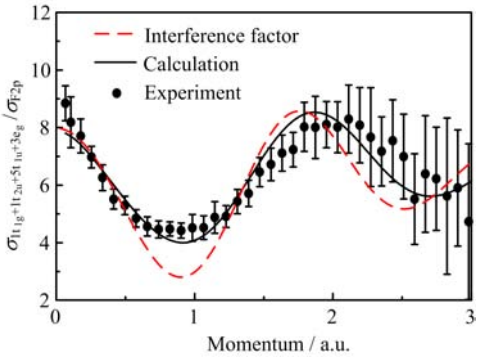

FIG. 4 Ratio of EMS cross sections of MOs to that of F2p AO and the corresponding interference factor for the summation of $1t_{1g}$, $1t_{2u}$+$5t_{1u}$, and $3e_g$.

with the corresponding interference factor. As can be seen in the figure, a good agreement between the experimental and theoretical ratios, as well as the interference factor, are achieved, further confirming the presence of the interference effect.

DOI:10.1063/1674-0068/28/cjcp1508168

IV. CONCLUSION

We report the highly sensitive EMS measurement on binding energy spectra and electron momentum profiles for the outer-valence molecular orbitals of SF_6. The experimental results are interpreted on the basis of the quantitative calculations using the density functional theory with B3LYP hybrid functional. Furthermore, for the four outermost F2p lone pair orbitals, the interference patterns are observed clearly through dividing the electron momentum profile of molecular orbitals by that of atomic F2p orbital. It clearly shows that EMS is a feasible experimental tool to directly investigate the interference effect even for the complicated species.

V. ACKNOWLEDGMENTS

This work was supported by the National Natural Science Foundation of China (No.11534011, No.11327404, and No.U1432118) and the Natural Science Research Programme of Education Department of Anhui Province (No.KJ1013A260).

[1] I. E. McCarthy and E. Weigold, Rep. Prog. Phys. **54**, 789 (1991).
[2] C. E. Brion, Int. J. Quant. Chem. **29**, 1397 (1986).
[3] M. A. Coplan, J. H. Moore, and J. P. Doering, Rev. Mod. Phys. **66**, 985 (1994).
[4] E. Weigold and I. E. McCarthy, *Electron Momentum Spectroscopy*, New York: Kluwer Academic/Plenum Pulblishers, (1999).
[5] J. P. D. Cook and C. E. Brion, Chem. Phys. **69**, 339 (1982).
[6] K. T. Leung and C. E. Brion, Chem. Phys. **91**, 43 (1984).
[7] N. Watanabe, X. J. Chen, and M. Takahashi, Phys. Rev. Lett. **108**, 173201 (2012).
[8] Z. Zhang, X. Shan, T. Wang, E. Wang, and X. J. Chen, Phys. Rev. Lett. **112**, 023204 (2014).
[9] M. Yamazaki, H. Satoh, N. Watanabe, D. B. Jones, and M. Takahashi, Phys. Rev. A **90**, 052711 (2014).
[10] A. Giardini-Guidoni, R. Fantoni, R. Tiribelli, D. Vinciguerra, R. Camilloni, and G. Stefani, J. Chem. Phys. **71**, 3182 (1979).
[11] E. Weigold, Y. Zheng, and W. von Niesscn, Chem. Phys. **150**, 405 (1991).
[12] Q. G. Tian, K. D. Wang, X. Shan, and X. J. Chen, Rev. Sci. Instrum. **82**, 033110 (2011).
[13] Q. G. Tian, *Ph.D. Dissertation*, Hefei: University of Science and Technology China, No.1012324243, (2012).
[14] C. Møller and M. S. Plesset, Phys. Rev. **46**, 0618 (1934).
[15] R. A. Kendall, T. H. Dunning, and R. J. Harrison, J. Chem. Phys. **96**, 6796 (1992).
[16] C. Lee, W. Yang, and R. G. Parr, Phys. Rev. B **37**, 785 (1988).
[17] A. D. Becke, J. Chem. Phys. **98**, 5648 (1993).
[18] P. Duffy, D. P. Chong, M. E. Casida, and D. R. Salahub, Phys. Rev. A **50**, 4707 (1994).
[19] M. E. Casida, Phys. Rev. A **51**, 2005 (1995).
[20] M. J. Frisch, G. W. Trucks, H. B. Schlegel, G. E. Scuseria, M. A. Robb, J. R. Cheeseman, J. A. Jr. Montgomery, T. Vreven, K. N. Kudin, J. C. Burant, J. M. Millam, S. S. Iyengar, J. Tomasi, V. Barone, B. Mennucci, M. Cossi, G. Scalmani, N. Rega, G. A. Petersson, H. Nakatsuji, M. Hada, M. Ehara, K. Toyota, R. Fukuda, J. Hasegawa, M. Ishida, T. Nakajima, Y. Honda, O. Kitao, H. Nakai, M. Klene, X. Li, J. E. Knox, H. P. Hratchian, J. B. Cross, C. Adamo, J. Jaramillo, R. Gomperts, R. E. Stratmann, O. Yazyev, A. J. Austin, R. Cammi, C. Pomelli, J. W. Ochterski, P. Y. Ayala, K. Morokuma, G. A. Voth, P. Salvador, J. J. Dannenberg, V. G. Zakrzewski, S. Dapprich, A. D. Daniels, M. C. Strain, O. Farkas, D. K. Malick, A. D. Rabuck, K. Raghavachari, J. B. Foresman, J. V. Ortiz, Q. Cui, A. G. Baboul, S. Clifford, J. Cioslowski, B. B. Stefanov, G. Liu, A. Liashenko, P. Piskorz, I. Komaromi, R. L. Martin, D. J. Fox, T. Keith, M. A. Al-Laham, C. Y. Peng, A. Nanayakkara, M. Challacombe, P. M. W. Gill, B. Johnson, W. Chen, M. W. Wong, C. Gonzalez, and J. A. Pople, *Gaussian 03, Revision B.04*, Pittsburgh PA: Gaussian Inc., (2003).
[21] D. M. P. Holland, M. A. MacDonald, P. Baltzer, L. Karlsson, M. Lundqvist, B. Wannberg, and W. von Niessen, Chem. Phys. **192**, 333 (1995).
[22] P. Duffy, M. E. Cassida, C. E. Brion, and D. P. Chong, Chem. Phys. **159**, 347 (1992).
[23] C. E. Brion, Y. Zheng, J. Rolke, J. J. Neville, I. E. McCarthy, and J. J. Wang, J. Phys. B **31**, L223 (1998).
[24] I. V. Litvinyuk, Y. Zheng, and C. E. Brion, Chem. Phys. **253**, 41 (2000).
[25] M. Takahashi, T. Saito, J. Hiraka, and Y. Udagawa, J. Phys. B **36**, 2539 (2003).
[26] X. G. Ren, C. G. Ning, J. K. Deng, S. F. Zhang, G. L. Su, F. Huang, and G. Q. Li, Phys. Rev. Lett. **94**, 163201 (2005)
[27] Y. R. Miao, J. K. Deng, and C. G. Ning, J. Chem. Phys. **136**, 124302 (2012).
[28] N. Watanabe, M. Yamazaki, and M. Takahashi, J. Chem. Phys. **137**, 114301 (2012).
[29] S. H. R. Shojaei, F. Morini, and M. S. Deleuze, J. Phys. Chem. A **117**, 1918 (2013).
[30] J. Yang, X. Shan, Z. Zhang, Y. Tang, M. Zhao, and X. J. Chen, J. Phys. Chem. A **118**, 11780 (2014).
[31] I. E. McCarthy, Aust. J. Phys. **48**, 1 (1995).
[32] L. S. Bartell, S. K. Doun, and S. R. Goates, J. Chem. Phys. **70**, 4585 (1979).

DOI:10.1063/1674-0068/28/cjcp1508168